Article

TiO₂/Au/TiO₂ Plasmonic Photocatalysts: The Influence of Titania Matrix and Gold Properties

Kenta Yoshiiri [1,2]**, Kunlei Wang** [2,3] **and Ewa Kowalska** [1,2,*]

1 Graduate School of Environmental Science, Hokkaido University, Sapporo 060-0808, Japan; yoshiiri@cat.hokudai.ac.jp
2 Institute for Catalysis (ICAT), Hokkaido University, Sapporo 060-0808, Japan; kunlei@cat.hokudai.ac.jp
3 Northwest Research Institute, Co., Ltd. of C.R.E.C., Lanzhou 730000, China
* Correspondence: kowalska@cat.hokudai.ac.jp

Abstract: Plasmonic photocatalysts have gained more and more attention because of possible applications for solar energy conversion, environmental decontamination, and water treatment. However, the activity under visible light is usually very low, and the property-governed activity as well as the mechanisms are not fully understood yet. Accordingly, this study examines four different titania photocatalysts (anatase and rutile with fine and large crystallites) modified with gold by photodeposition. Three kinds of samples were prepared, as follows: (i) gold-modified titania (Au/TiO₂), (ii) physically mixed Au/TiO₂ samples (Au/TiO₂(1) + Au/TiO₂(2)), and (iii) Au/(TiO₂(1) + Au/TiO₂(2)) samples, prepared by subsequent deposition of gold on the mixture of bare and gold-modified titania. In total, twelve samples were prepared and well characterized, including diffuse reflectance spectroscopy (DRS), X-ray diffraction (XRD), X-ray photoelectron spectroscopy (XPS), and scanning transmission electron microscopy (STEM). The photocatalytic activity was examined in three reaction systems: (i) methanol dehydrogenation during gold photodeposition under UV/vis irradiation, (ii) oxidative decomposition of acetic acid (UV/vis), and (iii) oxidation of 2-propanol to acetone under visible light irradiation (λ > 450 nm). It was found that during subsequent deposition, gold is mainly formed on the surface of pre-deposited Au nanoparticles (NPs), localized on fine titania NPs, through the electrostatic attractions (negatively charged gold resulting from photogenerated electrons' accumulation). This gold aggregation, though detrimental for UV activity (many "naked" large titania with low activity), is highly beneficial for vis activity because of efficient light harvesting and increased interface between gold and titania (gold deposits surrounded by fine titania NPs). Moreover, it was found that rutile is more active than anatase for plasmonic photocatalysis, probably due to easier electron transfer from gold via titania to adsorbed oxygen (more negative conduction band), which might hinder the back reaction (electron transfer: Au→TiO₂→Au).

Keywords: gold NPs; gold aggregation; photodeposition; plasmonic photocatalysis; titania

1. Introduction

Plasmonic photocatalysis, i.e., photocatalytic reactions initiated by plasmonic properties of metals, has been intensively studied since the first report by Tian and Tatsuma in 2005 on titania films loaded with gold nanoparticles (NPs) [1]. The main reason for huge interest in plasmonic photocatalysis is the ability to use the visible part of the solar spectrum, in contrast to the most active wide-bandgap semiconductor photocatalysts (mainly titania) with limited light harvesting ability (only UV light). Usually, plasmonic photocatalysts are composed of wide-bandgap semiconductors and NPs of noble metals (NMs) [2–4]. Although semiconductors modified with NMs have been well known and extensively investigated since Bard's studies in the 1970s, because of the improved photocatalytic activity resulting from the inhibition of charge carriers' recombination (NM working as an electron sink), the application of plasmonic feature of NMs is quite a new topic. Therefore, both the mechanism and the key factors of photocatalytic activities are still under debate [5–8].

The discussion on the former has focused mainly on two possibilities, i.e., an energy transfer [9–11] and an electron transfer ("hot"—plasmonic) [1,6,12–17]. Interestingly, it has been proposed that a slight change in the photocatalyst morphology could result in the change of the main mechanism [18]. The cleavage of chemical bonds due to plasmonic heating has also been proposed as the probable pathway of decomposition of chemical compounds [19,20], but again other reports have excluded such possibility [9,21]. Similarly, in the case of the property-governed activity, the contrary data have been presented, e.g., indicating that either fine or large NPs of NMs and/or semiconductors are recommended for high photocatalytic efficiency [2,3]. For example, a clear correlation has been found between the crystallite size of gold NPs (as well as titania) and photocatalytic activity for fifteen commercial titania samples modified with gold by photodeposition [14]. However, not only the size but also the high polydispersity of gold NPs seems to be the most crucial, allowing efficient light harvesting ability since the wavelength of localized surface plasmon resonance (LSPR) depends on the size and the shape of NPs. Accordingly, the most active samples are characterized but broad LSPR peak. The strategy of efficient light harvesting has also been achieved via preparation of multi-element photocatalysts (even named as "rainbow" [22]), such as bi-/tri-metallic [15,18,23–28] and hybrid (e.g., composed of plasmonic metal and ruthenium complexes [29,30] or metal oxides [31]) photocatalysts. Although multi-element photocatalysts are characterized by broad photoabsorption ability, a decrease in photocatalytic activity with respect to single modified semiconductors has also been observed, probably resulting from an extensive charge carriers' recombination on the second modifier instead of their transfer to the reactants [15,29,30,32].

It should be pointed out that plasmonic photocatalysts have already exhibited photocatalytic activities for numerous reactions, including degradation of pollutants in both liquid and gas phases, inactivation of microorganisms, water splitting, solar energy conversion, and synthesis of organic compounds [2,3,33]. However, the level of activity under vis irradiation is much lower than that under UV (even by a few orders in magnitude). Accordingly, various strategies have been proposed for the improvements of photocatalytic performance, including the preparation of multi-element photocatalysts (mentioned above), nanoarchitecture engineering (e.g., faceted NPs, nanotubes, nanowires, inverse opal photonic crystals [2,3,34–37]), and the design of efficient reaction systems, such as in the presence of electron donors and other materials allowing efficient charge transfer (e.g., via Z-scheme mechanism [26,38–40]) or hindering back reactions [41–43]. Moreover, the stability under vis irradiation might be also a problem, especially considering the mechanism of an electron transfer (e.g., from gold to titania). Indeed, discoloration of photocatalyst suspension has been observed during long-term vis irradiation, resulting from both gold aggregation (the metallic gold deposited on stirring bars) and oxidation [44]. Accordingly, it has been proposed that an increase in the interface between plasmonic NPs and wide-bandgap semiconductor might improve both the activity and the stability [45–47]. This strategy has been proven in our recent studies for gold-modified titania (of large/polydisperse gold particles and thus with broad LSPR peak and high vis activity) additionally surrounded by fine titania NPs [44]. For this study, large rutile and fine anatase with crystallite size of 517 and 11 nm, respectively, were used. However, it is impossible to conclude if and how the polymorphic form of titania might influence the photocatalytic performance. Therefore, here, four different titania samples of similar properties, i.e., both large and small (rutile and anatase), were examined as plasmonic photocatalysts, considering both titania and gold properties, as well as the interface between them.

2. Materials and Methods

2.1. Materials

Four commercial titania samples with similar properties, i.e., fine and large crystallites of anatase or rutile (ST F-10, MT-150A, ST41, and TKP-102, named as "R", "r", "A" and "a", where small and large letters mean small and large crystallite sizes, respectively) were used in this study. The properties of titania samples are shown in Table 1. Methanol, acetic acid,

2-propanol, acetone, and chloroauric acid ($HAuCl_4 \cdot 4H_2O$) (Wako Pure Chemical Industries, Ltd., Osaka, Japan) were used without further purification.

Table 1. The properties of commercial titania samples used in this study.

Name	Code	Supplier	Composition (%)			Crystallite Size */nm	SSA/m^2 g^{-1}	ETs/µmol g^{-1}
			Anatase	**Rutile**	**NC**			
ST F-10	R	Showa Denko Ceramics (Shiojiri, Japan)	4.0	93.0	3.0	60.6	13	55
MT-150A	r	Tayca (Osaka, Japan)	0.0	81.9	18.1	14.8	114	221
ST41	A	Ishihara Sangyo Kaisha (Osaka, Japan)	98.2	0.7	1.1	76.2	11	13
TKP-102	a	Tayca	89.3	0.0	10.7	16.7	114	77

* the crystallite size of major component; ETs—density of electron traps (data reported previously [48]); NC—non-crystalline phase; SSA—specific surface area (data reported previously [48]).

2.2. Photocatalyst Preparation

2.2.1. Simple Photodeposition Method of Gold on Titania (Au/TiO_2)

Au/TiO_2 photocatalysts (2 wt% of Au) were prepared by photodeposition method. One sample was prepared in six tubes (Pyrex, $\varphi 35 \times 96$ mm) (Corning, Inc., Corning, NY, USA) simultaneously to obtain ca. 3.5 g of photocatalyst (the irradiation system shown previously [49]). In each tube, titania powder (0.6 g) was suspended in methanol solution (28.6 mL; 50 vol%) by magnetic stirring and sonication (ultrasonic bath). Then, chloroauric acid ($HAuCl_4 \cdot 4H_2O$) aqueous solution (79 µM, 502 µL) was added under continuous stirring. The tube was purged of air with argon for at least 15 min and sealed off with a rubber septum. Then, the tubes were placed in a thermostated water bath (298 $\pm$ 5 K) and irradiated with a 400-W high-pressure mercury lamp ($\lambda > 290$ nm; lamp spectrum shown in SI [50]) under magnetic stirring (500 rpm) for 1 h. During irradiation, amount of generated hydrogen (methanol dehydrogenation) was measured every 15 min by gas chromatography (Shimadzu GC-8AIT (Kyoto, Japan) with TCD: Thermal Conductivity Detector, column: MS-5A, mobile phase: Ar). The thus-obtained Au/TiO_2 photocatalyst was centrifuged, washed at least three times with methanol and distilled water, dried overnight at 393 K, and ground in an agate mortar.

2.2.2. Preparation of $TiO_2/Au/TiO_2$ Photocatalysts

$TiO_2/Au/TiO_2$ photocatalysts were prepared by two methods, i.e., (1) simple physical mixing and (2) subsequent gold photodeposition, as follows.

(1) Physical mixing of two gold-modified samples containing both fine and large titania crystals was carried out by mild grounding of 80 wt% of Au/TiO_2 (large) with 20 wt% of Au/TiO_2 (fine) in an agate mortar. These samples are named as "($Au/TiO_2 + Au/TiO_2$)", where "R", "r", "A", and "a" are used according to the selected TiO_2. For example, (Au/R + Au/r) means the sample prepared by physical mixing of two gold-modified rutile samples containing large (80 wt%) and fine (20 wt%) rutile crystallites.

(2) Subsequent photodeposition is defined as gold deposition on the mixture of bare and gold-modified titania samples. Various combinations of titania were tested (same as those in the case of simple physical mixing), and obtained samples were named as "$Au/(TiO_2(1) + Au/TiO_2(2))$", i.e., gold was deposited on the mixture of bare titania (1) and gold-modified titania (2). The codes of "R", "r", "A", and "a" are used in the sample names respective to the selected titania (instead of $TiO_2(1)$ and $TiO_2(2)$).

Photocatalyst Characterization

The obtained samples were characterized by several techniques, including diffuse reflectance spectroscopy (DRS), X-ray diffraction (XRD), X-ray photoelectron spectroscopy (XPS), and scanning transmission electron microscopy (STEM; both TEM and SEM images

could be observed simultaneously for the same sample area.). The photoabsorption properties of samples were characterized by UV/vis DRS (JASCO V-670, Oklahoma City, OK, USA) using $BaSO_4$ as a reference. Crystalline properties were analyzed by XRD (Rigaku intelligent XRD SmartLab (Tokyo, Japan) with a Cu target). The surface properties were measured by XPS (JEOL JP-9010MC, Akishima, Japan) for 50 scans to estimate the oxidation state of titanium, oxygen, and gold. The morphology of samples was investigated by STEM (Hitachi HD2000, Tokyo, Japan) with three different modes: SE, ZC, and TE for secondary electron image, Z contrast image, and phase contrast image, respectively.

Photocatalytic Activity Testing

The photocatalytic activity was investigated in three reaction systems: (1) methanol dehydrogenation (during gold deposition) under UV/vis irradiation by Hg lamp ($\lambda > 290$ nm) in the absence of oxygen, (2) oxidative decomposition of acetic acid under UV/vis irradiation by Hg lamp (same setup as that for methanol dehydrogenation except the sample holder and sample tubes [49]), and (3) oxidation of 2-propanol to acetone for vis-activity testing with Xe lamp, cold mirror, and cut-off filter ($\lambda > 450$ nm). The irradiation system for vis activity testing could be found in the previous reports, e.g., [51]. For photocatalytic activity tests, 50 mg of sample was suspended in aqueous solution of methanol (50 vol%), acetic acid (5 vol%), or 2-propanol (5 vol%), and irradiated under continuous stirring. The amount of generated hydrogen and carbon dioxide was analyzed using a gas-chromatograph (GC-TCD; column: MS-5A, mobile phase: Ar), whereas acetone by GC with a flame ionization detector (GC-FID; column: PEG-20M (uniportB), mobile phase: N_2).

3. Results

3.1. Preparation of Gold-Modified Titania Samples

The photodeposition method, used here for the preparation of gold-modified titania samples, has many advantages, such as (i) short duration, (ii) efficient contact between gold and titania, (iii) complete deposition of metal precursor, and (iv) the ability to investigate the photocatalytic activity during metal deposition (as shown in Figure 1). In the case of gold-modified titania samples, gold cations are reduced by photogenerated electrons on the titania surface within several minutes, as clearly shown by linear evolution of hydrogen after short induction time (5.1–6.7 min in this study) in Figure 1a. The induction time depends on the properties of titania (and metal type), and usually correlates well with obtained photocatalytic activity, i.e., the shorter the induction time is, the higher is the photocatalytic activity (reaction rate) [52]. Of course, there is no induction time in the case of gold deposition on the mixture of bare and gold-modified titania (as shown for Au/(A + Au/a)) since there is already gold in the system on which hydrogen molecules could be formed. It should be mentioned that pristine titania is practically inactive for hydrogen evolution, and thus a co-catalyst (e.g., gold) must be used. The complete deposition of whole metal precursor has already been proven by flame atomic absorption spectroscopy for the large range of gold content (0.05–10 wt%) in the previous study [53].

The summarized data of photocatalytic activity (reaction rate of hydrogen evolution) during gold deposition are shown in Figure 1b. In the case of Au/TiO_2 samples (with only one type of titania), the photocatalytic activity dropped in the following order: Au/R > Au/a > Au/r > Au/A, i.e., the highest activity was obtained for large rutile and fine anatase. Similar data have already been presented for different commercial titania samples modified with gold [50] and silver [49]. Based on these data and also another study for 35 titania photocatalysts tested for various reactions (including also methanol dehydrogenation with in-situ platinum deposition) [54], it might be proposed that large specific surface area and high crystallinity (low content of non-crystalline phase and low content of electron traps (ETs), as shown in Table 1) are crucial factors for efficient hydrogen generation on anatase- and rutile-based gold-modified samples, respectively.
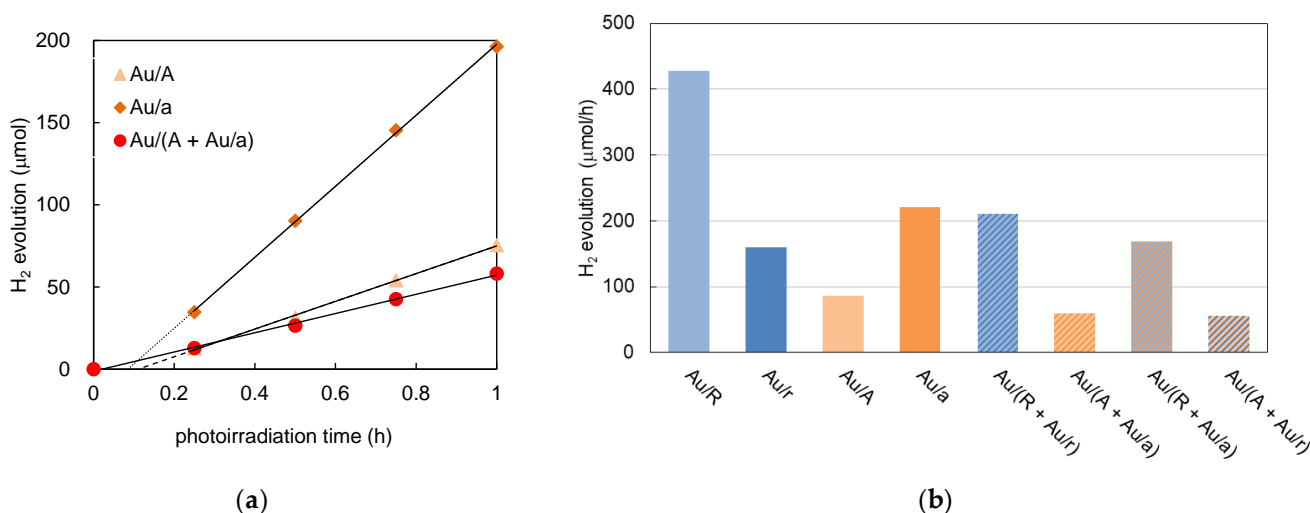
Figure 1. The reaction rates of hydrogen evolution during gold photodeposition on titania samples: (**a**) Time-dependent activity for three exemplary samples: Au/A, Au/a, and Au/(A + Au/a); (**b**) data for all samples prepared by photodeposition.

The most surprising is unexpectedly low activities for $TiO_2/Au/TiO_2$ samples, which are much lower than the expected data (the weighted average of its component, i.e., 80% of large titania (Au/R or Au/A) and 20% of fine titania (Au/r or Au/a)). Moreover, three samples show even lower activity than both their components. Therefore, it is clear that the properties of gold NPs must have been different from that in Au/TiO_2 photocatalysts, prepared by simple photodeposition. It is proposed that during the second photodeposition, gold is mainly deposited on pre-deposited gold NPs (on fine titania) since NMs work as an electron pool, and thus under irradiation, photogenerated electrons from titania are accumulated on the gold deposits. Accordingly, gold NPs should be negatively charged, facilitating the adsorption of gold cations on them. A similar observation has been noticed in the case of bi-metallic titania, in which copper was photodeposited on the surface of pre-deposited silver [32]. Therefore, the formation of larger gold NPs mainly on the fine titania surface causes that there are many non-modified titania samples with negligible activity. This aspect has been well discussed for platinum-modified titania, where it has been shown that the most important is deposition of platinum on every titania particle [55].

3.2. Properties of Au/TiO₂ and TiO₂/Au/TiO₂ Samples

The morphology of samples was observed by STEM, and exemplary images are shown in Figure 2, whereas the distribution of gold NPs' size for four different samples, i.e., Au/R, Au/r, (Au/R + Au/r), and Au/(R + Au/r), is in Figure 3. It is clear that much larger NPs are formed on larger titania, which agrees with previous findings [14,50]. It has been proposed that gold is preferably formed on the surface defects [56], and fine titania is characterized by larger content of defects (observed clearly as ETs, Table 1) [48,57]. Accordingly, a large number of fine gold NPs could be found on titania with fine NPs. In contrast, high crystallization of titania with large NPs results in formation of larger gold NPs because of gold aggregation, as shown in Figure 2c. Interestingly, two $TiO_2/Au/TiO_2$ samples prepared by different methods (physical mixing and subsequent deposition) are characterized by quite different properties. Obviously, the physically mixed sample (Au/R + Au/r) exhibits the resultant properties from both its components. However, the Au/(R + Au/r) sample consists of larger NPs than those in Au/r but also without the largest NPs (>90 nm) observed in Au/R. Indeed, as suggested from the activity data during methanol dehydrogenation (Figure 1), it might be proposed that gold NPs pre-deposited on fine rutile are working as gold seeds, which are growing during subsequent photodeposition.
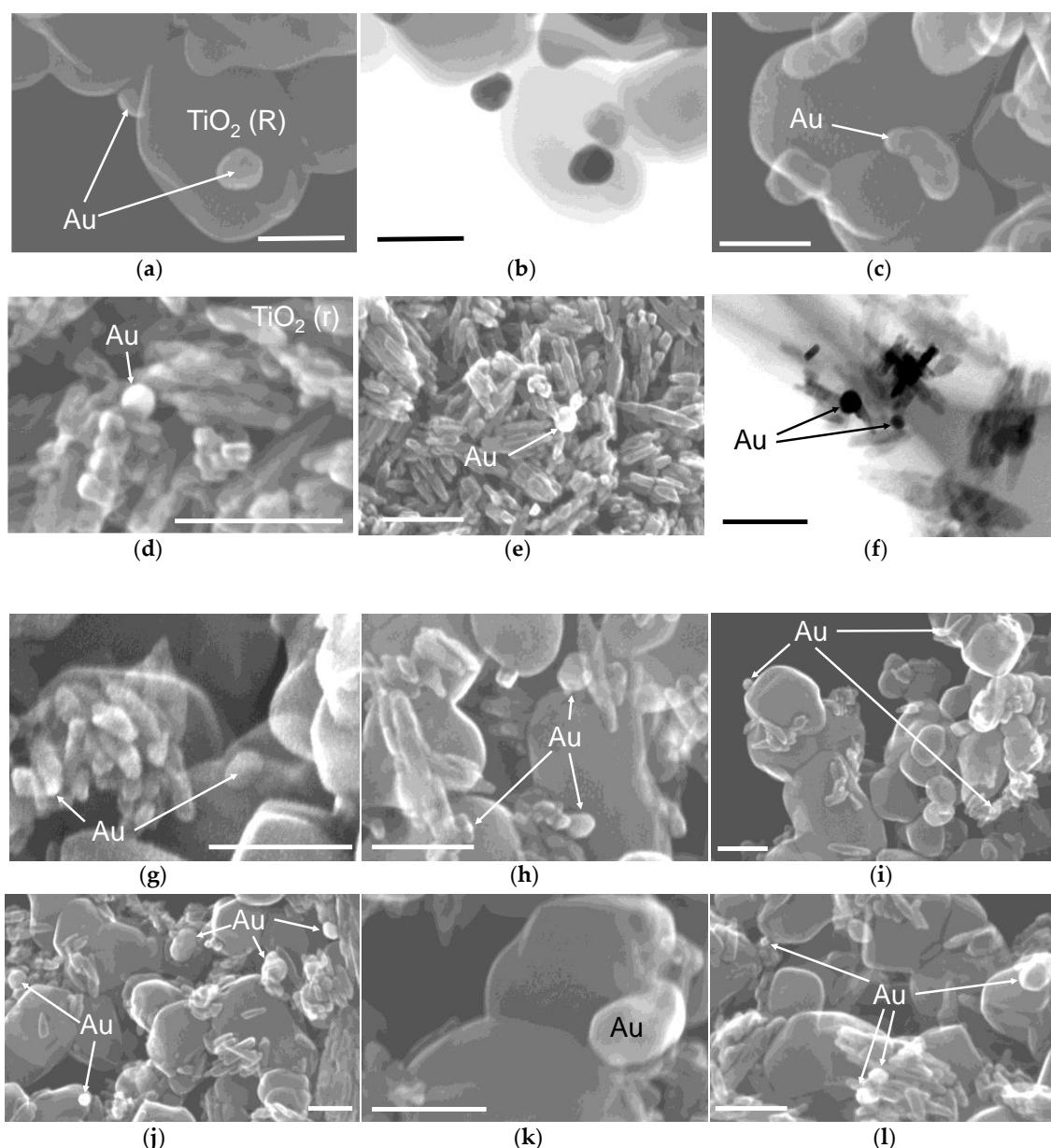
Figure 2. STEM images of: (**a**–**c**) Au/R; (**d**–**f**) Au/r; (**g**–**i**) (Au/R + Au/r); (**j**–**l**) Au/(R + Au/r); SE mode for all images except of TE for (**b**) and (**f**). The images at (**a**) and (**b**) show the same area of Au/R sample. Scale bars correspond to 100 nm.

The exemplary STEM images (Figure 2) clearly show that much larger gold NPs are formed on large (a–c) than small (d–f) titania samples. The aggregated (composed of small NPs) gold deposit is easily observed in image c, forming a "kidney"-like structure. The sample prepared by physical mixing consists of gold NPs deposited on both fine and large titania. In contrast, in the case of subsequent photodeposition, gold NPs are mainly found next to fine rutile NPs, confirming the possible "seed growth" of gold during subsequent photoirradiation.

The photoabsorption properties of all samples are shown in Figure 4. Obviously, there is no vis response in the case of pristine titania samples due to their wide bandgap. The difference in photoabsorption edge between titania polymorphs is clearly seen in Figure 4c,d, resulting from the narrower bandgap of rutile than anatase. The deposition of gold on the titania surface has caused the appearance of vis response for all modified samples. The position of LSPR peak depends on gold NPs' size/shape [58–60], and thus

bathochromic shift is clearly observed with an increase in gold size and any deviations from the spherical shape. Accordingly, the LSPR peak appears at the longest wavelengths for Au/R sample with the largest gold NPs of not only spherical morphology (e.g., elongated—Figure 2c). The summary of LSPR wavelengths (at max intensity) is presented in Table 2. As expected, all samples prepared by subsequent deposition exhibit LSPR peak at shorter wavelengths than samples obtained by physical mixing, i.e., confirming smaller size of gold NPs, which results from the predominant deposition of gold on pre-deposited gold NPs located on the particles of fine titania (less gold deposited on large titania).
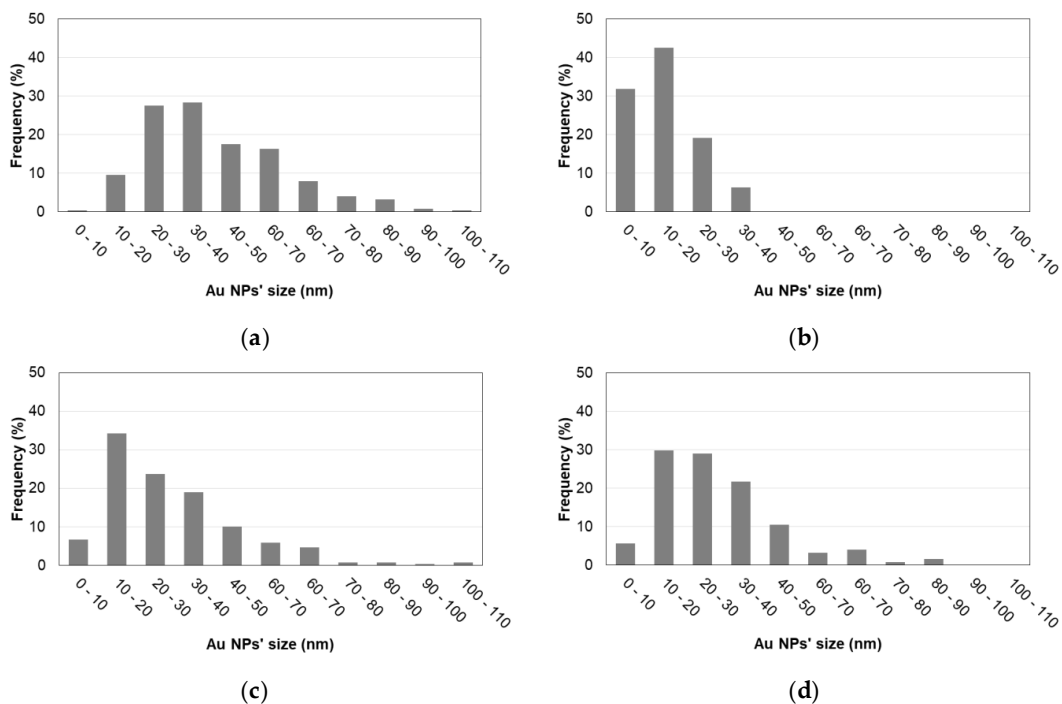

Figure 3. The distribution of gold NPs' size in gold-modified titania samples: (**a**) Au/R; (**b**) Au/r; (**c**) (Au/R + Au/r); (**d**) Au/(R + Au/r).
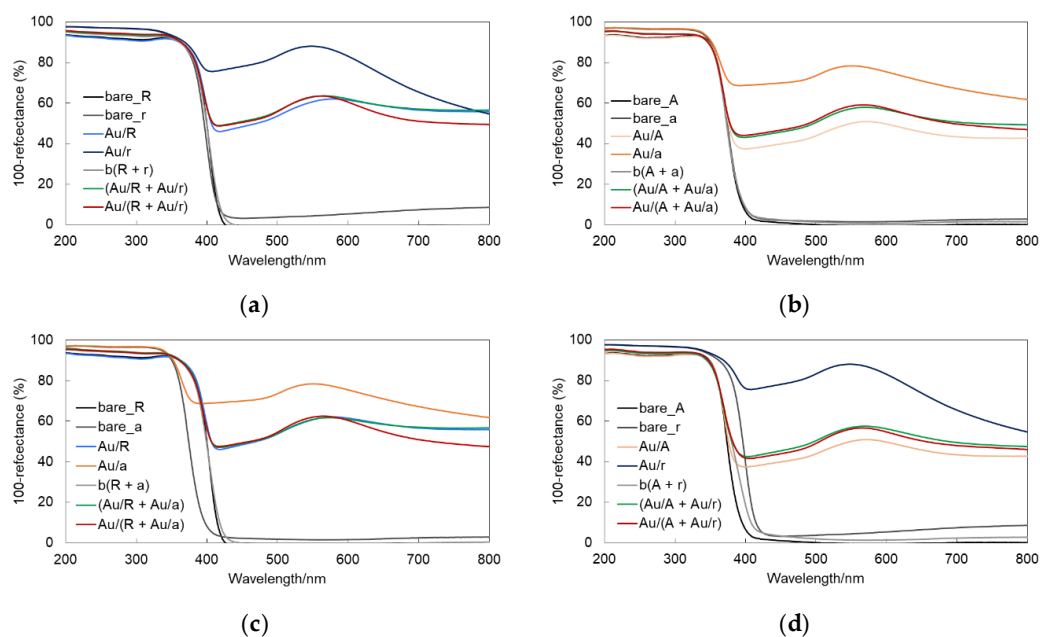

Figure 4. DRS data for bare and gold-modified titania samples taken with $BaSO_4$ as a reference for bare and gold-modified samples containing: (**a**) R and r; (**b**) A and a; (**c**) R and a; (**d**) A and r.

Table 2. Photoabsorption properties of gold deposits in $TiO_2/Au/TiO_2$ samples (LSPR wavelength at max intensity).

Sample Code $TiO_2(1) + TiO_2(2)$	LSPR Peak/nm			
	$TiO_2(1)$	$TiO_2(2)$	$(Au/TiO_2(1) + Au/TiO_2(2))$	$Au/(TiO_2(1) + Au/TiO_2(2))$
R + r	578	549	567	562
A + a	572	550	571	569
R + a	578	550	573	565
A + r	572	549	569	566

For further characterization of samples, crystalline properties were analyzed, and obtained data are presented in Table 3 and Figure 5. Titania polymorphs were confirmed in all samples, i.e., rutile in R- and r-based-samples, and anatase in A- and a-based photocatalysts. The slight content of anatase and rutile in R and A, reaching 7.0% and 0.5%, respectively, has also been found. The co-existence of titania polymorphs in commercial products is common, resulting from a simple transition from metastable anatase to stable rutile at higher temperatures. Moreover, any impurities during titania synthesis could result in the change of transformation temperature. For example, lattice constraint might cause the destabilization or stabilization, depending on the size, valence, and content effects, and thus inhibiting or accelerating the phase transition [61]. The large content of impurities (above the solubility limit) might result in their precipitation, facilitating the phase transition via heterogeneous nucleation [62]. Additionally, small content of anatase could be stabilized by non-crystalline phase, impurities, co-existing other phases (mutual phase stabilization via an interfacial reaction mechanism), and special morphology (e.g., faceted NPs) [63–65]. A size-dependent transition has also been proposed [66]. Moreover, amorphous titania is also present even in the case of samples thermally treated at temperatures higher than 500 °C [55,67]. Therefore, almost all commercial products are composed of two or more titania forms, mainly anatase, rutile, and amorphous titania.

Table 3. Crystalline composition and crystallite sizes of titania and gold in gold-modified titania samples.

Sample	Crystallite Size (nm)			Crystalline Composition (%)		
	Anatase	Rutile	Gold	Anatase	Rutile	Gold
Au/R	38.7	60.4	24.6	6.6	91.2	2.3
Au/r		14.8	18.9	0.0	97.7	2.3
Au/A	76.2	103.6	31.1	97.5	0.5	2.0
Au/a	16.7		13.7	97.7	0.0	2.3
(Au/R + Au/r)	40.2	63.0	24.5	5.4	92.2	2.4
Au/(R + Au/r)	39.3	62.9	20.5	5.5	92.2	2.3
(Au/A + Au/a)	86.6	131.9	27.4	96.8	1.2	2.0
Au/(A + Au/a)	89.5	76.0	23.3	94.8	3.2	2.0
(Au/R + Au/a)	23.0	60.2	26.7	23.3	74.4	2.3
Au/(R + Au/a)	23.8	60.5	23.3	22.3	75.5	2.2
(Au/A + Au/r)	77.9	16.9	30.9	80.6	17.3	2.1
Au/(A + Au/r)	79.9	17.5	27.3	81.6	16.4	2.0

The crystallite sizes of titania (considering the main phase) correlate with specific surface area (Table 1) and STEM observation, i.e., reaching 60.4, 14.8, 76.2, and 16.7 nm for R, r, A, and a, respectively. Gold has been detected in all samples, and its content correlates well with that used for photodeposition (2 wt%). The crystallite sizes of gold correspond well to DRS and STEM data, i.e., the titania properties influence the size of formed gold NPs, and thus the largest and the smallest gold deposits have been formed in Au/R and Au/a samples, respectively. Like data of LSPR wavelength, the subsequent deposition of gold results in the formation of smaller crystallites than those obtained by

physical mixing. Obviously, the crystallite sizes in the case of samples prepared by physical mixing corresponds to the weighted average of gold diameter (23.5, 27.6, 22.4, and 28.6 nm for (Au/R + Au/r), (Au/A + Au/a), (Au/R + Au/a), and (Au/A + Au/r), respectively) obtained from its component, i.e., 80% Au/large titania and 20% Au/fine titania.
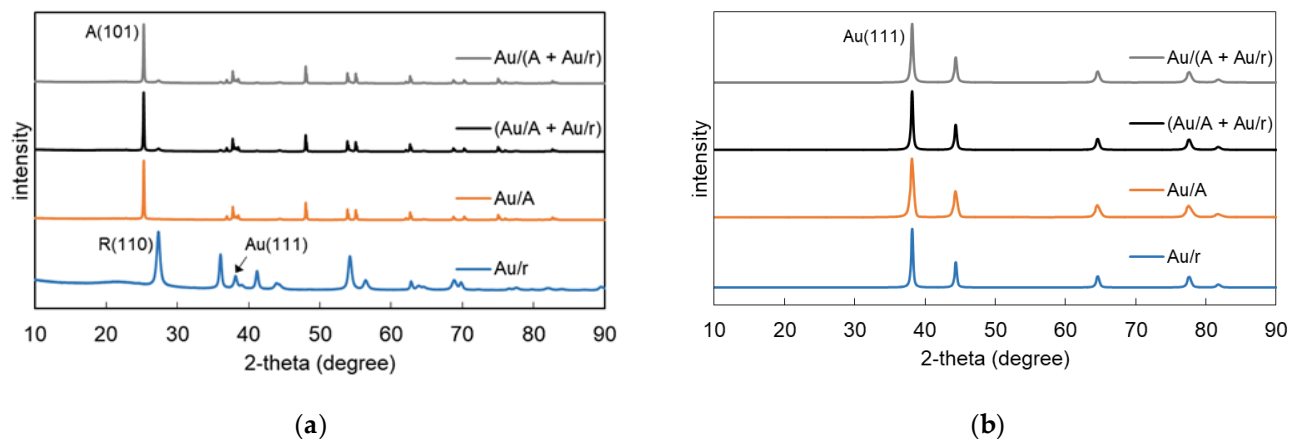

(**a**)　　　　　　　　　　　　　　　　　　　　　(**b**)

Figure 5. XRD data for Au/r, Au/A, (Au/A + Au/r), and Au/(A + Au/r): (**a**) original results; (**b**) data showing gold peaks (after subtraction of titania peaks).

For surface characterization, XPS analysis was performed for selected samples, and obtained data are shown in Figure 6 and Table 4. Three elements were investigated, i.e., titanium, oxygen, and gold, based on Ti $2p_{3/2}$, O 1s, and Au 4 $f_{7/2}$, respectively. The binding energies were analyzed after deconvolution of respective XPS peaks in accordance with the literature [68–71]. Gold on the surface exists predominantly in zero-valent state in all samples, ranging from 57% to 92%, and thus correlating well with observed plasmonic properties. Interestingly, the lowest (57%) and the largest (80%) contents of zero-valent gold in Au/TiO$_2$ samples were obtained for Au/R and Au/r, respectively. It is thought that in the case of fine titania samples, titania could partly cover the surface of gold NPs (Figure 2d–f), thus resulting in its stabilization. In contrast, on large and well crystallized titania particles, many "naked" gold NPs are observed (Figure 2a–c). Therefore, it is not surprising that TiO$_2$/Au/TiO$_2$ samples possess much larger content of zero-valent gold that Au/R. The oxygen peak could be divided into three peaks at ca. 528, 530.5, and 532.5 eV, indicating the presence of: (i) oxygen in TiO$_2$, (ii) Ti$_2$O$_3$, C=O, and hydroxyl groups bound to two titanium atoms, and (iii) OH groups bound to carbon and/or titanium, respectively [71]. Interestingly, the lowest content of hydroxyl groups is observed in TiO$_2$/Au/TiO$_2$ samples, especially those prepared by physical mixing, which suggests that hydroxyl groups participated in the connection between two kinds of Au/TiO$_2$ photocatalysts. It has already been shown that Ti-OH sites readily bound oxides [72] and metal NPs/clusters, including gold (Au-O) [73]. Moreover, an oxygen-rich surface has been suggested as the most recommended for efficient and stable adsorption of gold on the titania surface, forming Au-O bonds with Au 5d-O 2p hybridization and charge transfer like gold-oxides [74]. In the case of titanium, its main form is Ti^{4+} (86–94%), which is obvious considering the chemical formula of titania. The presence of the reduced form of titanium is common for various titania photocatalysts. As already reported [75], photodeposition of gold on the titania surface resulted in an increase in the content of trivalent titanium from 9.3 to 12% (R vs. Au/R), which is reasonable considering highly reductive conditions during the reaction (photogenerated electrons, anaerobic conditions, methanol as a hole scavenger). Interestingly, the content of Ti^{3+} is much larger in the case of the samples prepared by physical mixing than subsequent deposition. This could be caused by the preferential deposition of gold on the pre-deposited Au NPs localized on the surface of fine titania (as suggested from hydrogen evolution data, STEM, and DRS), and thus a predominant part of titania (<less than 80%) is without gold NPs but under strong reductive conditions.
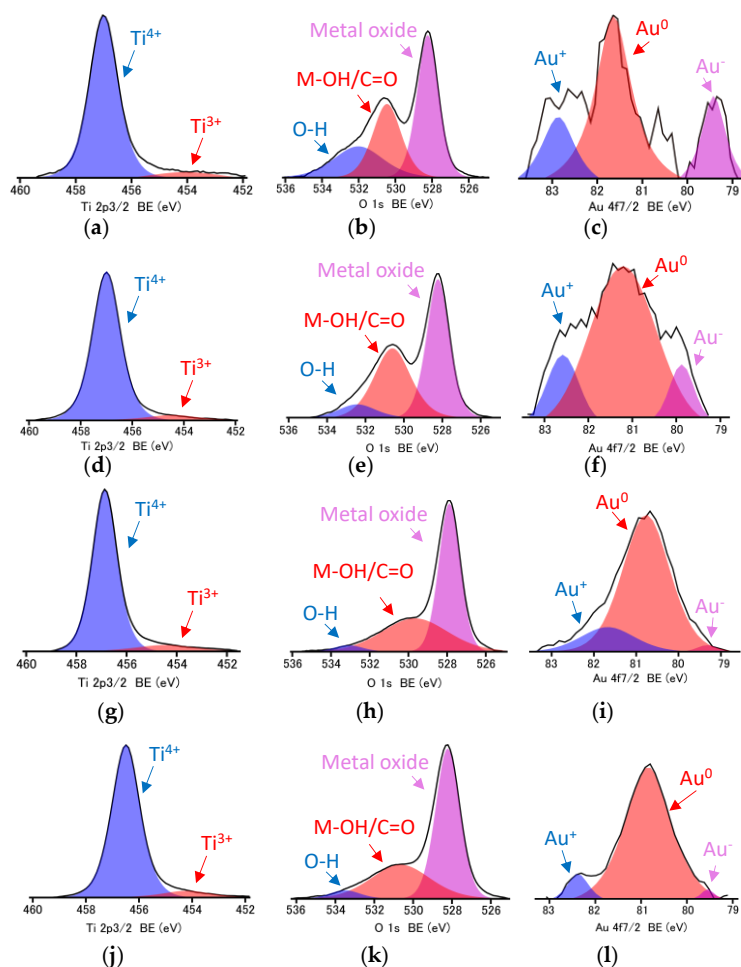
Figure 6. XPS data for: (**a–c**) Au/R; (**d–f**) Au/a; (**g–i**) (Au/R + Au/a); (**j–l**) Au/(R + Au/a) samples; for deconvoluted peaks of: (**a,d,g,j**) titanium (Ti $2p_{3/2}$), (**b,e,h,k**) oxygen (O 1s), and (**c,f,i,l**) gold (Au $4f_{7/2}$).

Table 4. The surface composition of titanium, oxygen, and gold in gold-modified titania samples.

Sample	Titanium (%)		Oxygen (%)			Gold (%)		
	Ti^{4+}	Ti^{3+}	OH	CO/M-OH	TiO$_2$	Au$^+$	Au^0	Au$^-$
Au/R	88.0	12.0	24.0	27.9	48.1	22.0	56.9	21.1
Au/r	94.0	6.0	15.4	40.8	43.8	10.9	79.9	9.2
Au/a	94.4	5.6	8.7	41.1	50.2	15.2	75.3	9.5
(Au/R + Au/r)	85.8	14.2	3.2	31.1	65.7	10.1	80.5	9.4
Au/(R + Au/r)	94.0	6.0	12.9	42.5	44.6	20.3	68.6	11.1
(Au/R + Au/a)	89.5	10.5	1.3	43.0	55.7	17.7	81.0	1.3
Au/(R + Au/a)	93.2	6.8	2.5	36.7	60.8	7.0	91.6	1.4

3.3. Photocatalytic Activity under UV/Vis and Vis Irradiation by Au/TiO$_2$ and TiO$_2$/Au/TiO$_2$ Photocatalysts

The photocatalytic activity was investigated (in addition to hydrogen evolution data shown in Section 3.1) for oxidative decomposition of acetic acid and 2-propanol under UV/vis and vis irradiation, respectively.

Figure 7 presents photocatalytic activity data for CO$_2$ evolution during acetic acid decomposition. In the case of bare titania samples, the activity increases in the following order: r < R < a < A. The higher activity of anatase, especially for oxidation reactions, are well known, and might result from both more positive level of valence band (stronger oxidation power by photogenerated holes [76]) and higher mobility of photogenerated charges (slower recombination) [67]. Interestingly, titania samples with larger particles

(both anatase and rutile) show higher activity in contrast to common knowledge, i.e., the larger the specific surface area is, the higher is the efficiency [54]. It is possible that the density of ETs, being the possible recombination centers, could play the crucial role. Indeed, the lowest and the highest ETs densities are in A and r samples, respectively (Table 1). The modification with gold enhanced activity significantly for three samples, i.e., Au/A, Au/a, and Au/R, with the highest enhancement for large rutile. It should be pointed out that under UV irradiation, photogenerated electrons migrate to gold NPs, inhibiting their recombination with holes. Therefore, samples with higher rate of charge carriers' recombination (usually rutile) should benefit the most. Interestingly, no activity enhancement has been observed for Au/r sample. It might be proposed that this sample, characterized by the largest density of ETs, is hardly active at all because of fast charge carriers' recombination. Then, modification with gold results in the preparation of violet sample containing only limited number of titania NPs in the direct contact with gold deposits (Figure 2d–f). Accordingly, even if gold can scavenge the photogenerated electrons, its contact with titania is insufficient (numerous bare titania), and additionally, gold might cause a "shielding effect", i.e., competing with titania for photons. Accordingly, even a slight decrease in activity was observed. It should be mentioned that usually, deposition of NMs results in significant activity enhancement under UV irradiation [50,52,77–80]. However, there are also some reports showing that NMs could decrease photocatalytic activity [81–84]. In our previous study on gold-modified titania for fifteen titania photocatalysts, only one sample showed a slight decrease in activity, whereas in the case of all other photocatalysts, the activity increased significantly (1.7–4.8 times) [50]. Interestingly, the sample with decreased activity was very similar to the present one, i.e., fine rutile (TIO6 from Catalysis Society of Japan) of 15-nm crystallites and high ETs density of 152 μmol g^{-1} [48].
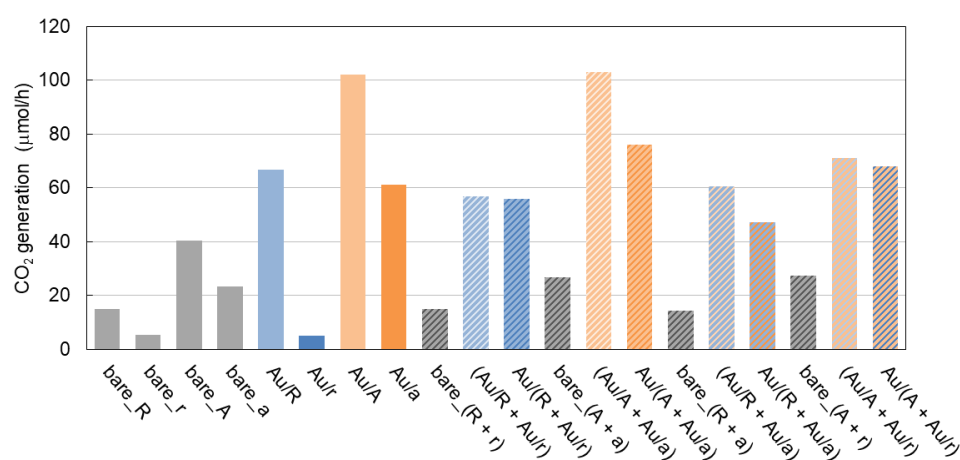

Figure 7. The photocatalytic activity of bare and gold-modified titania samples under UV/vis for oxidative decomposition of acetic acid.

In the case of TiO_2/Au/TiO_2 samples, unfortunately no activity improvement could be observed. This could result from the competitive photon absorption [55] by two Au/TiO_2 components. Accordingly, some photons are absorbed by less active Au/TiO_2 (smaller titania) instead of highly active gold-modified titania with large particles. Interestingly, all samples prepared by physical mixing are less active than corresponding samples prepared by subsequent photodeposition. This is further proof that the properties of gold have been changed. Therefore, the mixture of fine titania with aggregated gold and less active bare titania of large particles (preferable deposition of gold on Au/TiO_2) is much less active than the mixture of two types of gold-modified samples.

Next, the photocatalytic activity under vis irradiation was analyzed, and obtained data are shown in Figure 8. As expected, in the case of Au/TiO_2 samples, the highest activity was obtained for Au/R, because of the broadest LSPR peak, resulting from the highest polydispersity of gold deposits in this sample, and thus efficient use of photons

with different energies. However, the most interesting is that the second most active sample is not Au/A with also broad LSPR peak, but Au/r (the least active under UV, Figure 6) with fine gold deposits of similar sizes. The study on fifteen Au/TiO$_2$ samples also showed the highest activity of rutile-based photocatalysts, but it was concluded that probably the properties of gold are the most crucial (linear increase in activity with gold size increase) [50]. However, here, the opposite behavior for Au/r and Au/A with the lowest and the highest activity under UV, respectively, suggests that rutile phase could be crucial for vis response of plasmonic photocatalysts. Interestingly, other studies on coupled semiconductors (Cu$_2$O/TiO$_2$) show similar tendency, i.e., the composite containing the fine rutile (TIO6) with the worst activity under UV is the most activity under vis [85]. It has been proposed that the difference in the redox potential of the excited electrons (conduction band; CB) between anatase and rutile could be responsible for this behavior. Considering the more negative value of CB for rutile than anatase, the charge transfer from CB of cuprous oxide to CB of titania could be facilitated. Similarly, considering an electron transfer mechanism for plasmonic photocatalysts, more negative CB of rutile could be beneficial for lower possibility of back electron transfer, as a result of easier reduction of adsorbed oxygen (more efficient O$_2{}^{\bullet-}$ generation [76]).
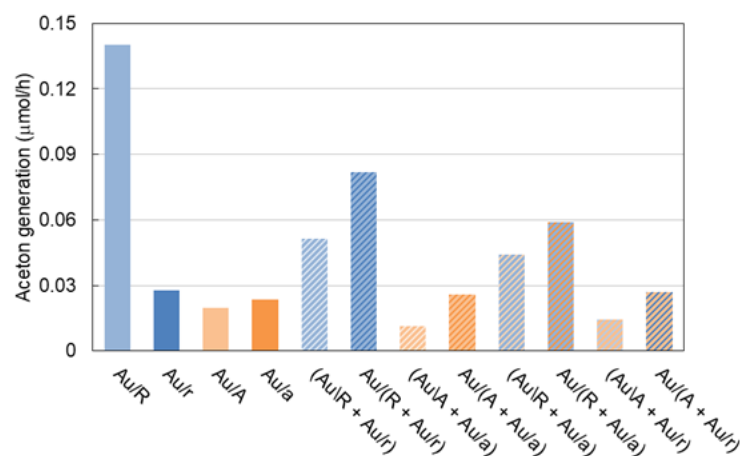

Figure 8. The photocatalytic activity of gold-modified titania samples under vis for oxidative decomposition of 2-propanol.

For TiO$_2$/Au/TiO$_2$ samples, the highest activity was obtained for the samples containing large rutile. Unfortunately, in contrast to previous study on similar materials (TiO$_2$/Au/TiO$_2$) [44], no activity enhancement in respect to Au/R could be obtained. It is thought that probably different ratio of components should be used since in the previous study, the rutile of much larger particles (>500 nm) was used, and the contents of large rutile and fine anatase were experimentally optimized. Interestingly, in contrast to UV activity, all samples prepared by physical mixing exhibit lower activity than respective photocatalysts obtained by subsequent photodeposition. There are two possible explanations. First, the larger interface between gold and titania, as gold is mainly formed on pre-deposited gold NPs (on fine titania), and thus many titania NPs could be in contact with gold deposits, as already suggested in the previous study [44]. Secondly, the larger and more polydisperse gold NPs could harvest light more efficiently. However, the latter is not so obvious, considering the hypsochromic shift of LSPR and the lack of the largest gold NPs (in respect to physically mixed samples). Accordingly, it is thought that the interface between gold and titania is the most crucial for efficient electron transfer. Moreover, it has been proposed that the plasmon-induced oxidation reactions take place at the active sites localized at the interface between gold and titania [86]. Therefore, the interface seems to be crucial for the overall redox reactions, i.e., both electron transfer from gold to titania (reductive pathway) and oxidation reactions.

4. Summary and Conclusions

Plasmonic photocatalysts composed of titania and gold NPs could be easily prepared by photodeposition method. Although the photocatalytic activity of $TiO_2/Au/TiO_2$ samples was not improved under UV or vis irradiation (in respect to their Au/TiO_2 components), many interesting findings were obtained in this study, as follows.

First, it was proven that the modification of titania with gold NPs might significantly enhance UV activity, and also result in appearance of vis response.

Second, the properties of titania as well as its polymorphic forms significantly influence the resultant properties of gold deposits and the overall activity.

Third, it was found that during subsequent photodeposition, gold is likely to adsorb through the electrostatic attractions on the surface of pre-deposited gold NPs on fine titania.

Fourth, the rutile phase was shown to be most active for vis activity, probably due to more negative position of CB than that in anatase, which might hinder the back electron transfer ($Au{\rightarrow}TiO_2{\rightarrow}Au$) as electrons could be easier scavenged by adsorbed oxygen.

Fifth, although the photodeposition method has many advantages, including short duration, complete deposition, good contact (interface), and ability to investigate the progress of reaction in situ (hydrogen evolution), it is hardly possible to control the properties of gold deposits. Accordingly, NPs with high polydispersity in the size/shape could be formed, and though being beneficial for vis activity, it is not recommended for the clarification of the key factors of efficiency. Nevertheless, it might be concluded that the aggregation of gold (e.g., during subsequent photodeposition) has a dual effect: (1) It is not recommended for UV activity since it causes the preparation of photocatalysts with many "naked" titania particles (and thus with low activity) that are competing for photons with Au/TiO_2 particles; (2) it is highly recommended for vis response due to efficient absorption of photons (broad LSPR peak) as well as larger interface when aggregated gold is in the vicinity of many fine titania NPs.

Author Contributions: Conceptualization, E.K.; methodology, E.K.; investigation, K.Y. and K.W.; resources, E.K.; writing—original draft preparation, K.Y. and K.W.; writing—review and editing, E.K.; visualization, K.Y. and K.W.; supervision, E.K.; funding acquisition, E.K. All authors have read and agreed to the published version of the manuscript.

Data Availability Statement: The data presented in this study are available on request from corresponding author (E.K.).

Conflicts of Interest: The authors declare no conflict of interest.

References

1. Tian, Y.; Tatsuma, T. Mechanisms and Applications of Plasmon-Induced Charge Separation at TiO_2 Films Loaded with Gold Nanoparticles. *J. Am. Chem. Soc.* **2005**, *127*, 7632–7637. [CrossRef] [PubMed]
2. Raja-Mogan, T.; Ohtani, B.; Kowalska, E. Photonic crystals for plasmonic photocatalysis. *Catalysts* **2020**, *10*, 827. [CrossRef]
3. Wei, Z.; Janczarek, M.; Wang, K.; Zheng, S.; Kowalska, E. Morphology-governed performance of plasmonic photocatalysts. *Catalysts* **2020**, *10*, 1070. [CrossRef]
4. Verbruggen, S.W. TiO_2 photocatalysis for the degradation of pollutants in gas phase: From morphological design to plasmonic enhancement. *J. Photochem. Photobiol. C* **2015**, *24*, 64–82. [CrossRef]
5. Asapu, R.; Claes, N.; Ciocarlan, R.G.; Minjauw, M.; Detavernier, C.; Cool, P.; Bals, S.; Verbruggen, S.W. Electron Transfer and Near-Field Mechanisms in Plasmonic Gold-Nanoparticle-Modified TiO_2 Photocatalytic Systems. *ACS Appl. Nano Mater.* **2019**, *2*, 4067–4074. [CrossRef]
6. Caretti, I.; Keulemans, M.; Verbruggen, S.W.; Lenaerts, S.; Van Doorslaer, S. Light-Induced Processes in Plasmonic Gold/TiO_2 Photocatalysts Studied by Electron Paramagnetic Resonance. *Top. Catal.* **2015**, *58*, 776–782. [CrossRef]

7. Brennan, L.J.; Purcell-Milton, F.; Salmeron, A.S.; Zhang, H.; Govorov, A.O.; Fedorov, A.V.; Gun'ko, Y.K. Hot plasmonic electrons for generation of enhanced photocurrent in gold-TiO_2 nanocomposites. *Nanoscale Res. Lett.* **2015**, *10*, 38. [CrossRef]

8. Ueno, K.; Misawa, H. Surface plasmon-enhanced photochemical reactions. *J. Photochem. Photobiol. C* **2013**, *15*, 31–52. [CrossRef]

9. Cushing, S.K.; Li, J.T.; Meng, F.K.; Senty, T.R.; Suri, S.; Zhi, M.J.; Li, M.; Bristow, A.D.; Wu, N.Q. Photocatalytic Activity Enhanced by Plasmonic Resonant Energy Transfer from Metal to Semiconductor. *J. Am. Chem. Soc.* **2012**, *134*, 15033–15041. [CrossRef]

10. Li, J.; Cushing, S.K.; Meng, F.; Senty, T.R.; Bristow, A.D.; Wu, N. Plasmon-induced resonance energy transfer for solar energy conversion. *Nat. Photon.* **2015**, *9*, 601–607. [CrossRef]

11. Ingram, D.B.; Christopher, P.; Bauer, J.L.; Linic, S. Predictive Model for the Design of Plasmonic Metal/Semiconductor Composite Photocatalysts. *ACS Catal.* **2011**, *1*, 1441–1447. [CrossRef]

12. Sakai, N.; Fujiwara, Y.; Takahashi, Y.; Tatsuma, T. Plasmon-resonance-based generation of cathodic photocurrent at electrode-posited gold nanoparticles coated with TiO_2 films. *ChemPhysChem* **2009**, *10*, 766–769. [CrossRef] [PubMed]

13. Furube, A.; Du, L.; Hara, K.; Katoh, R.; Tachiya, M. Ulltrafast plasmon-induced electron transfer from gold nanodots into TiO_2 nanoparticles. *J. Am. Chem. Soc.* **2007**, *129*, 14852–14853. [CrossRef]

14. Kowalska, E.; Abe, R.; Ohtani, B. Visible light-induced photocatalytic reaction of gold-modified titanium(IV) oxide particles: Action spectrum analysis. *Chem. Commun.* **2009**, *2*, 241–243. [CrossRef] [PubMed]

15. Kowalska, E.; Janczarek, M.; Rosa, L.; Juodkazi, S.; Ohtani, B. Mono- and bi-metallic plasmonic photocatalysts for degradation of organic compounds under UV and visible light irradiation. *Catal. Today* **2014**, *230*, 131–137. [CrossRef]

16. Kominami, H.; Tanaka, A.; Hashimoto, K. Mineralization of organic acids in aqueous suspension of gold nanoparticles supported on cerium(IV) oxide powder under visible light irradiation. *Chem. Commun.* **2010**, *46*, 1287–1289. [CrossRef]

17. Priebe, J.B.; Radnik, J.; Lennox, A.J.J.; Pohl, M.M.; Karnahl, M.; Hollmann, D.; Grabow, K.; Bentrup, U.; Junge, H.; Beller, M.; et al. Solar Hydrogen Production by Plasmonic Au-TiO_2 Catalysts: Impact of Synthesis Protocol and TiO_2 Phase on Charge Transfer Efficiency and H_2 Evolution Rates. *ACS Catal.* **2015**, *5*, 2137–2148. [CrossRef]

18. Horiguchi, Y.; Kanda, T.; Torigoe, K.; Sakai, H.; Abe, M. Preparation of Gold/Silver/Titania Trilayered Nanorods and Their Photocatalytic Activities. *Langmuir* **2014**, *30*, 922–928. [CrossRef]

19. Chen, X.; Zhu, H.-Y.; Zhao, J.-C.; Zheng, Z.-F.; Gao, X.-P. Visible-light-driven oxidation of organic contaminants in air with gold nanoparticle catalysts on oxide supports. *Angew. Chem. Int. Ed.* **2008**, *47*, 5353–5356. [CrossRef]

20. Wang, C.J.; Ranasingha, O.; Natesakhawat, S.; Ohodnicki, P.R.; Andio, M.; Lewis, J.P.; Matranga, C. Visible light plasmonic heating of Au-ZnO for the catalytic reduction of CO_2. *Nanoscale* **2013**, *5*, 6968–6974. [CrossRef]

21. Kominami, H.; Tanaka, A.; Hashimoto, K. Gold nanoparticles supported on cerium(IV) oxide powder for mineralization of organic acids in aqueous suspensions under irradiation of visible light of λ = 530 nm. *Appl. Catal. A Gen.* **2011**, *397*, 121–126. [CrossRef]

22. Verbruggen, S.W.; Keulemans, M.; Goris, B.; Blommaerts, N.; Bals, S.; Martens, J.A.; Lenaerts, S. Plasmonic 'rainbow' photocatalyst with broadband solar light response for environmental applications. *Appl. Catal. B Environ.* **2016**, *188*, 147–153. [CrossRef]

23. Malankowska, A.; Kobylanski, M.P.; Mikolajczyk, A.; Cavdar, O.; Nowaczyk, G.; Jarek, M.; Lisowski, W.; Michalska, M.; Kowalska, E.; Ohtani, B.; et al. TiO_2 and $NaTaO_3$ Decorated by Trimetallic Au/Pd/Pt Core-Shell Nanoparticles as Efficient Photocatalysts: Experimental and Computational Studies. *ACS Sustain. Chem. Eng.* **2018**, *6*, 16665–16682. [CrossRef]

24. Zielinska-Jurek, A.; Wei, Z.; Wysocka, I.; Szweda, P.; Kowalska, E. The effect of nanoparticles size on photocatalytic and antimicrobial properties of Ag-Pt/TiO_2 photocatalysts. *Appl. Surf. Sci.* **2015**, *353*, 317–325. [CrossRef]

25. Zielińska-Jurek, A.; Kowalska, E.; Sobczak, J.W.; Lisowski, W.; Ohtani, B.; Zaleska, A. Preparation and characterization of monometallic (Au) and bimetallic (Ag/Au) modified-titania photocatalysts activated by visible light. *Appl. Catal. B Environ.* **2011**, *101*, 504–514. [CrossRef]

26. Bielan, Z.; Kowalska, E.; Dudziak, S.; Wang, K.; Ohtani, B.; Zielinska-Jurek, A. Mono- and bimetallic (Pt/Cu) titanium(IV) oxide core–shell photocatalysts with UV/Vis light activity and magnetic separability. *Catal. Today* **2021**, *361*, 198–209. [CrossRef]

27. Verma, P.; Yuan, K.; Kuwahara, Y.; Mori, K.; Yamashita, H. Enhancement of plasmonic activity by Pt/Ag bimetallic nanocatalyst supported on mesoporous silica in the hydrogen production from hydrogen storage material. *Appl. Catal. B Environ.* **2018**, *223*, 10–15. [CrossRef]

28. Quiroz, J.; Barbosa, E.C.M.; Araujo, T.P.; Fiorio, J.L.; Wang, Y.-C.; Zou, Y.-C.; Mou, T.; Alves, T.V.; de Oliveira, D.C.; Wang, B.; et al. Controlling Reaction Selectivity over Hybrid Plasmonic Nanocatalysts. *Nano Lett.* **2018**, *18*, 7289–7297. [CrossRef]

29. Zheng, S.; Wei, Z.; Yoshiiri, K.; Braumuller, M.; Ohtani, B.; Rau, S.; Kowalska, E. Titania modification with ruthenium(II) complex and gold nanoparticles for photocatalytic degradation of organic compounds. *Photochem. Photobiol. Sci.* **2016**, *15*, 69–79. [CrossRef]

30. Kowalska, E.; Yoshiiri, K.; Wei, Z.; Zheng, S.; Kastl, E.; Remita, H.; Ohtani, B.; Rau, S. Hybrid photocatalysts composed of titania modified with plasmonic nanoparticles and ruthenium complexes for decomposition of organic compounds. *Appl. Catal. B Environ.* **2015**, *178*, 133–143. [CrossRef]

31. Mendez-Medrano, M.G.; Kowalska, E.; Lehoux, A.; Herissan, A.; Ohtani, B.; Bahena, D.; Briois, V.; Colbeau-Justin, C.; Rodriguez-Lopez, J.; Remita, H. Surface modification of TiO_2 with Ag nanoparticles and CuO nanoclusters for applications in photocatalysis. *J. Phys. Chem. C* **2016**, *120*, 5143–5154. [CrossRef]

32. Janczarek, M.; Wei, Z.; Endo, M.; Ohtani, B.; Kowalska, E. Silver- and copper-modified decahedral anatase tiania particles as visible light-responsive plasmonic photocatalyst. *J. Photon. Energy* **2017**, *7*, 012008. [CrossRef]

33. Endo-Kimura, M.; Kowalska, E. Plasmonic Photocatalysts for Microbiological Applications. *Catalysts* **2020**, *10*, 824. [CrossRef]

34. Bian, Z.F.; Tachikawa, T.; Zhang, P.; Fujitsuka, M.; Majima, T. Au/TiO$_2$ Superstructure-Based Plasmonic Photocatalysts Exhibiting Efficient Charge Separation and Unprecedented Activity. *J. Am. Chem. Soc.* **2014**, *136*, 458–465. [CrossRef] [PubMed]

35. Lv, C.; Wang, L.L.; Liu, X.G.; Zhao, L.; Lan, X.F.; Shi, J.S. An efficient inverse opal (IO)-TiO$_2$-MoO$_{3-x}$ for photocatalytic H$_2$ evolution and RhB degradation—The synergy effect of IO structure and plasmonic MoO$_{3-x}$. *Appl. Surf. Sci.* **2020**, *527*, 146726. [CrossRef]

36. Bian, J.; Qu, Y.; Zhang, X.L.; Sun, N.; Tang, D.Y.; Jing, L.Q. Dimension-matched plasmonic Au/TiO$_2$/BiVO$_4$ nanocomposites as efficient wide-visible-light photocatalysts to convert CO$_2$ and mechanistic insights. *J. Mater. Chem. A* **2018**, *6*, 11838–11845. [CrossRef]

37. Shi, J.; Chen, J.; Li, G.; An, T.; Yamashita, H. Fabrication of Au/TiO$_2$ nanowires@carbon fiber paper ternary composite for visible-light photocatalytic degradation of gaseous styrene. *Catal. Today* **2017**, *281*, 621–629. [CrossRef]

38. Zhang, Z.; Huang, J.; Fang, Y.; Zhang, M.; Liu, K.; Dong, B. A Nonmetal Plasmonic Z-Scheme Photocatalyst with UV- to NIR-Driven Photocatalytic Protons Reduction. *Adv. Mater.* **2017**, *29*, 1606688. [CrossRef]

39. Wang, S.; Gao, Y.; Qi, Y.; Li, A.; Fan, F.; Li, C. Achieving overall water splitting on plasmon-based solid Z-scheme photocatalysts free of redox mediators. *J. Catal.* **2017**, *354*, 250–257. [CrossRef]

40. Li, X.; Jin, Y.; Dou, Z.; Zhou, S.; Zhang, Q.; Bao, N. Rational design of Z-scheme Bi$_{12}$O$_{17}$Cl$_2$/plasmonic Ag/anoxic TiO$_2$ composites for efficient visible light photocatalysis. *Powder Technol.* **2021**, *384*, 342–352. [CrossRef]

41. Fudo, E.; Tanaka, A.; Kominami, H. Bifunctions of a Cr hydroxide layer for water splitting over a platinized Au/TiO$_2$ plasmonic photocatalyst under visible light irradiation. *Catal. Today*, 2022, *in press*. [CrossRef]

42. Shaik, F.; Peer, I.; Jain, P.K.; Amirav, L. Plasmon-Enhanced Multicarrier Photocatalysis. *Nano Lett.* **2018**, *18*, 4370–4376. [CrossRef] [PubMed]

43. Ghobadi, T.G.U.; Ghobadi, A.; Ozbay, E.; Karadas, F. Strategies for Plasmonic Hot-Electron-Driven Photoelectrochemical Water Splitting. *ChemPhotoChem* **2018**, *2*, 161–182. [CrossRef]

44. Wang, K.; Yoshiiri, K.; Rosa, L.; Wei, Z.; Juodkazis, S.; Ohtani, B.; Kowalska, E. TiO$_2$/Au/TiO$_2$ plasmonic photocatalyst with enhanced photocatalytic activity and stability under visible-light irradiation. *Catal. Today* **2022**, *397–399*, 257–264. [CrossRef]

45. Peeters, H.; Keulemans, M.; Nuyts, G.; Vanmeert, F.; Li, C.; Minjauw, M.; Detavernier, C.; Bals, S.; Lenaerts, S.; Verbruggen, S.W. Plasmonic gold-embedded TiO$_2$ thin films as photocatalytic self-cleaning coatings. *Appl. Catal. B Environ.* **2020**, *267*, 8. [CrossRef]

46. Ahlawat, M.; Mittal, D.; Rao, V.G. Plasmon-induced hot-hole generation and extraction at nano-heterointerfaces for photocatalysis. *Commun. Mater.* **2021**, *2*, 114. [CrossRef]

47. Kim, J.; Son, H.Y.; Nam, Y.S. Multilayered Plasmonic Heterostructure of Gold and Titania Nanoparticles for Solar Fuel Production. *Sci. Rep.* **2018**, *8*, 10464. [CrossRef]

48. Nitta, A.; Takase, M.; Takashima, M.; Murakamid, N.; Ohtani, B. A fingerprint of metal-oxide powders: Energy-resolved distribution of electron traps. *Chem. Commun.* **2016**, *52*, 12096–12099. [CrossRef]

49. Yoshiiri, K.; Karabiyik, B.; Wang, K.; Wei, Z.; Colbeau-Justin, C.; Kowalska, E. The property-governed activity of silver-modified titania photocatalysts: The influence of titania matrix. *J. Chem. Phys.* 2022; *in press*. [CrossRef]

50. Kowalska, E.; Mahaney, O.O.P.; Abe, R.; Ohtani, B. Visible-light-induced photocatalysis through surface plasmon excitation of gold on titania surfaces. *Phys. Chem. Chem. Phys.* **2010**, *12*, 2344–2355. [CrossRef]

51. Kowalska, E.; Rau, S. Photoreactors for wastewater treatment: A review. *Recent Pat. Eng.* **2010**, *4*, 242–266. [CrossRef]

52. Wei, Z.; Endo, M.; Wang, K.; Charbit, E.; Markowska-Szczupak, A.; Ohtani, B.; Kowalska, E. Noble metal-modified octahedral anatase titania particles with enhanced activity for decomposition of chemical and microbiological pollutants. *Chem. Eng. J.* **2017**, *318*, 121–134. [CrossRef]

53. Kowalska, E.; Rau, S.; Ohtani, B. Plasmonic Titania Photocatalysts Active under UV and Visible-Light Irradiation: Influence of Gold Amount, Size, and Shape. *J. Nanotechnol.* **2012**, *2012*, 361853. [CrossRef]

54. Prieto-Mahaney, O.O.; Murakami, N.; Abe, R.; Ohtani, B. Correlation between photocatalytic activities and structural and physical properties of titanium(IV) oxide powders. *Chem. Lett.* **2009**, *38*, 238–239. [CrossRef]

55. Wang, K.L.; Wei, Z.S.; Ohtani, B.; Kowalska, E. Interparticle electron transfer in methanol dehydrogenation on platinum-loaded titania particles prepared from P25. *Catal. Today* **2018**, *303*, 327–333. [CrossRef]

56. Min, B.K.; Wallace, W.T.; Goodman, D.W. Support effects on the nucleation, growth, and morphology of gold nano-clusters. *Surf. Sci.* **2006**, *600*, L7. [CrossRef]

57. Murakami, N.; Abe, R.; Ohtani, B. In situ observation of photocatalytic reaction by photoacoustic spectroscopy: Detection of heat of exothermic photocatalytic reaction. *Chem. Phys. Lett.* **2008**, *451*, 316–320. [CrossRef]

58. Xia, Y.N.; Halas, N.J. Shape-controlled synthesis and surface plasmonic properties of metallic nanostructures. *MRS Bull.* **2005**, *30*, 338–344. [CrossRef]

59. Zhu, J.; Huang, L.Q.; Zhao, J.W.; Wang, Y.C.; Zhao, Y.R.; Hao, L.M.; Lu, Y.M. Shape dependent resonance light scattering properties of gold nanorods. *Mater. Sci. Eng. B* **2005**, *121*, 199–203. [CrossRef]

60. Murazawa, N.; Ueono, K.; Mizeikis, V.; Juodkazis, S.; Misawa, H. Spatially Selective Nonlinear Photopolymerization Induced by the Near-Field of Surface Plasmons Localized on Rectangular Gold Nanorods. *J. Phys. Chem. C* **2009**, *113*, 1147–1149. [CrossRef]

61. Hanaor, D.A.H.; Sorrell, C.C. Review of the anatase to rutile phase transformation. *J. Mater. Sci.* **2011**, *46*, 855–874. [CrossRef]

62. Janes, R.; Knightley, L.J.; Harding, C.J. Structural and spectroscopic studies of iron (III) doped titania powders prepared by sol-gel synthesis and hydrothermal processing. *Dyes Pigments* **2004**, *62*, 199–212. [CrossRef]

63. Zhang, Q.; Li, C. High Temperature Stable Anatase Phase Titanium Dioxide Films Synthesized by Mist Chemical Vapor Deposition. *Nanomaterials* **2020**, *10*, 911. [CrossRef] [PubMed]

64. Janczarek, M.; Kowalska, E.; Ohtani, B. Decahedral-shaped anatase titania photocatalyst particles: Synthesis in a newly developed coaxial-flow gas-phase reactor. *Chem. Eng. J.* **2016**, *289*, 502–512. [CrossRef]

65. Debnath, R.; Chaudhuri, J. Mutual phase stabilization of aluminium phosphate and titania in AlPO$_4$-TiO$_2$ binary system. *Bull. Mater. Sci.* **1992**, *15*, 441–447. [CrossRef]

66. Satoh, N.; Nakashima, T.; Yamamoto, K. Metastability of anatase: Size dependent and irreversible anatase-rutile phase transition in atomic-level precise titania. *Sci. Rep.* **2013**, *3*, 1959. [CrossRef] [PubMed]

67. Wang, K.; Wei, Z.; Colbeau-Justin, C.; Nitta, A.; Kowalska, E. P25 and its components—Electronic properties and photocatalytic activities. *Surf. Interfaces* **2022**, *31*, 102057. [CrossRef]

68. Kruse, N.; Chenakin, S. XPS characterization of Au/TiO$_2$ catalysts: Binding energy assessment and irradiation effects. *Appl. Catal. A Gen.* **2011**, *391*, 367–376. [CrossRef]

69. Rossnagel, S.M.; Sites, J.R. X-ray photoelectron spectroscopy of ion beam sputter deposited silicon dioxide, titanium dioxide, and tantalum pentoxide. *J. Vac. Sci. Technol.* **1984**, *2*, 376–379. [CrossRef]

70. Jensen, H.; Soloviev, A.; Li, Z.S.; Sogaard, E.G. XPS and FTIR investigation of the surface properties of different prepared titania nano-powders. *Appl. Surf. Sci.* **2005**, *246*, 239–249. [CrossRef]

71. Yu, J.G.; Zhao, X.J.; Zhao, Q.N. Effect of surface structure on photocatalytic activity of TiO$_2$ thin films prepared by sol-gel method. *Thin Solid Films* **2000**, *379*, 7–14. [CrossRef]

72. Panayotov, D.; McEntee, M.; Burrows, S.; Driscoll, D.; Tang, W.; Neurock, M.; Morris, J. Infrared studies of propene and propene oxide adsorption on nanoparticulate Au/TiO$_2$. *Surf. Sci.* **2016**, *652*, 172–182. [CrossRef]

73. Chrétien, S.; Metiu, H. Density functional study of the interaction between small Au clusters, Au$_n$ (n = 1–7) and the rutile TiO$_2$ surface. I. Adsorption on the stoichiometric surface. *J. Chem. Phys.* **2007**, *127*, 084704. [CrossRef]

74. Shi, H.; Kohyama, M.; Tanaka, S.; Takeda, S. Structure and stability of Au rods on TiO$_2$(110) surfaces by first-principles calculations. *Phys. Rev. B* **2009**, *80*, 155413. [CrossRef]

75. Wei, Z.; Janczarek, M.; Endo, M.; Wang, K.L.; Balcytis, A.; Nitta, A.; Mendez-Medrano, M.G.; Colbeau-Justin, C.; Juodkazis, S.; Ohtani, B.; et al. Noble metal-modified faceted anatase titania photocatalysts: Octahedron versus decahedron. *Appl. Catal. B Environ.* **2018**, *237*, 574–587. [CrossRef] [PubMed]

76. Buchalska, M.; Kobielusz, M.; Matuszek, A.; Pacia, A.; Wojtyla, S.; Macyk, W. On Oxygen Activation at Rutile- and Anatase-TiO$_2$. *ACS Catal.* **2015**, *5*, 7424–7431. [CrossRef]

77. Pichat, P.; Mozzanega, M.N.; Disdier, J.; Herrmann, J.M. Platinum content and temperature effects on the photocatalytic hydrogen production from aliphatic alcohols over platinum/titanium dioxide. *Nouv. J. Chim.* **1982**, *6*, 559–564.

78. Nishimoto, S.I.; Ohtani, B.; Kagiya, T. Photocatalytic Dehydrogenation of Aliphatic-Alcohols by Aqueous Suspensions of Platinized Titanium-Dioxide. *J. Chem. Soc. Faraday Trans.* **1985**, *81*, 2467–2474. [CrossRef]

79. Sato, S.; White, J.M. Photodecomposition of water over platinum/titanium dioxide catalysts. *Chem. Phys. Lett.* **1980**, *72*, 83–86. [CrossRef]

80. Hussein, F.H.; Rudham, R. Photocatalytic dehydrogenation of liquid alcohols by platinized anatase. *J. Chem. Soc. Faraday Trans.* **1987**, *83*, 1631–1639. [CrossRef]

81. Gyulavári, T.; Kovács, K.; Kovács, Z.; Bárdos, E.; Kovács, G.; Baán, K.; Magyari, K.; Veréb, G.; Pap, Z.; Hernadi, K. Preparation and characterization of noble metal modified titanium dioxide hollow spheres—New insights concerning the light trapping efficiency. *Appl. Surf. Sci.* **2020**, *534*, 147327. [CrossRef]

82. Tóth, Z.-R.; Kovács, G.; Hernádi, K.; Baia, L.; Pap, Z. The investigation of the photocatalytic efficiency of spherical gold nanocages/TiO$_2$ and silver nanospheres/TiO$_2$ composites. *Sep. Purif. Technol.* **2017**, *183*, 216–225. [CrossRef]

83. Kovács, G.; Baia, L.; Vulpoi, A.; Radu, T.; Karácsonyi, É.; Dombi, A.; Hernádi, K.; Danciu, V.; Simon, S.; Pap, Z. TiO$_2$/WO$_3$/Au nanoarchitectures' photocatalytic activity, "from degradation intermediates to catalysts' structural peculiarities", Part I: Aeroxide P25 based composites. *Appl. Catal. B Environ.* **2014**, *147*, 508–517. [CrossRef]

84. Veréb, G.; Ambrus, Z.; Pap, Z.; Kmetykó, Á.; Dombi, A.; Danciu, V.; Cheesman, A.; Mogyorósi, K. Comparative study on UV and visible light sensitive bare and doped titanium dioxide photocatalysts for the decomposition of environmental pollutants in water. *Appl. Catal. A Gen.* **2012**, *417–418*, 26–36. [CrossRef]

85. Janczarek, M.; Endo, M.; Zhang, D.; Wang, K.; Kowalska, E. Enhanced photocatalytic and antimicrobial prformance of cuprous oxide/titania: The effect of titania matrix. *Materials* **2018**, *11*, 2069. [CrossRef]

86. Wang, S.; Gao, Y.; Miao, S.; Liu, T.; Mu, L.; Li, R.; Fan, F.; Li, C. Positioning the Water Oxidation Reaction Sites in Plasmonic Photocatalysts. *J. Am. Chem. Soc.* **2017**, *139*, 11771–11778. [CrossRef]